# Setting, Processing, and Stacking Velocities

# of the "Teal South" datasets

# from the Teal South Field

# Eugene Island Block 354

# Gulf of Mexico

David Forel

Seismic Rocks LLC

**Note:** The Teal South datasets available on seismicrocks.com were processed by a contractor. The prestack datasets are:
(a) NMO-corrected common midpoint or CMP (P-P wave) gathers and
(b) NMO-corrected common conversion point or CCP (P-S wave) gathers.

**Table of Contents**

## 1. Location and Data Acquisition

Teal South field is in the Gulf of Mexico, about 80 miles offshore, in Eugene Island Block 354 (Figure 1). The water depth is just under 90 meters.


*Figure 1. Location of Teal South field (map from Google).*

Teal South's multiple reservoirs of unconsolidated Tertiary sands produce both oil and gas from depths of 4000 ft to 8000 ft. (Ebrom et al., 1998).

In 1995, Texaco conducted a streamer survey (PP-waves only) in Teal South. This survey was done before production started in the Teal South field. The streamer data, which are not included, are called the Legacy data.

In July 1997, Texaco conducted a 4-component survey. (Four-component recording means that each receiver position has an inline geophone, a crossline geophone, a vertical geophone, and a hydrophone.) The July 1997 survey is called Phase 1. At the time of this survey, the 4500 ft sand had been in production for over eight months (Ebrom et al., 1998).

In late 1997, Texaco turned control of the project over to the Energy Research Clearing House (ERCH).

In April 1999 (21 months after Phase 1), ERCH coordinated another 4-component survey, Phase 2.

For both Phase 1 and Phase 2, source spacing was approximately 25m x 25 m. Phase 1 acquisition covered approximately 3000 m x 3000 m. Phase 2 acquisition covered approximately 4000 m x 3000 m. Figures 2 and 3 show source and ocean bottom cable (OBC) receiver locations for each phase. Figures 4 and 5 show cable relationships for each phase.

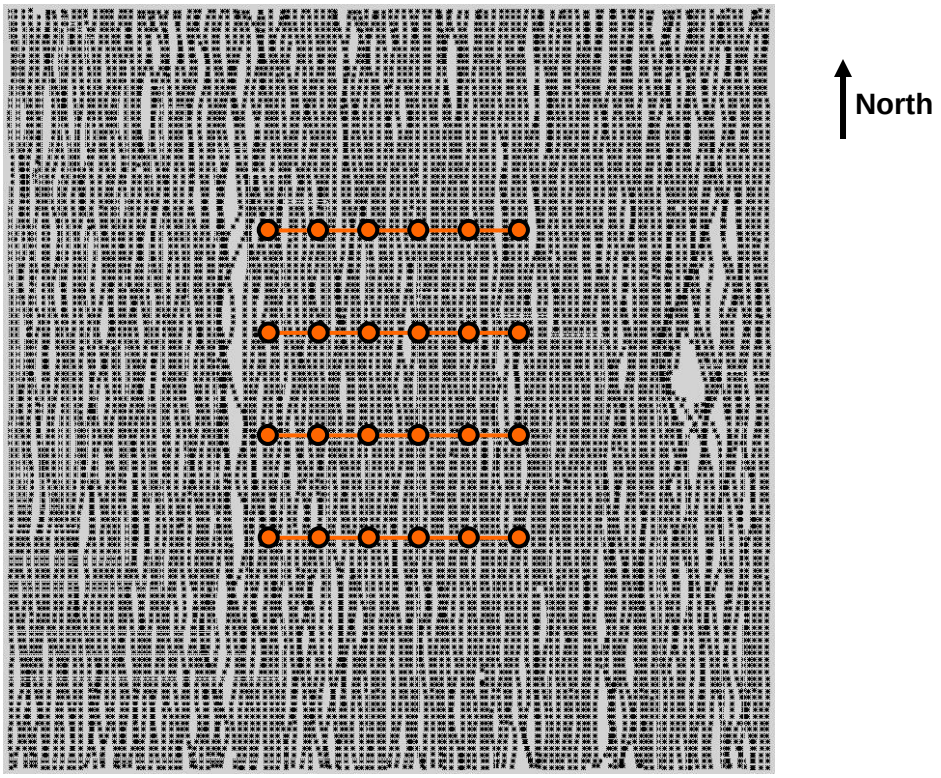


*Figure 2.* ***Phase 1****. Black squares show source positions, orange dots show receiver locations. Source positions covered approximately 3000 m x 3000 m.*

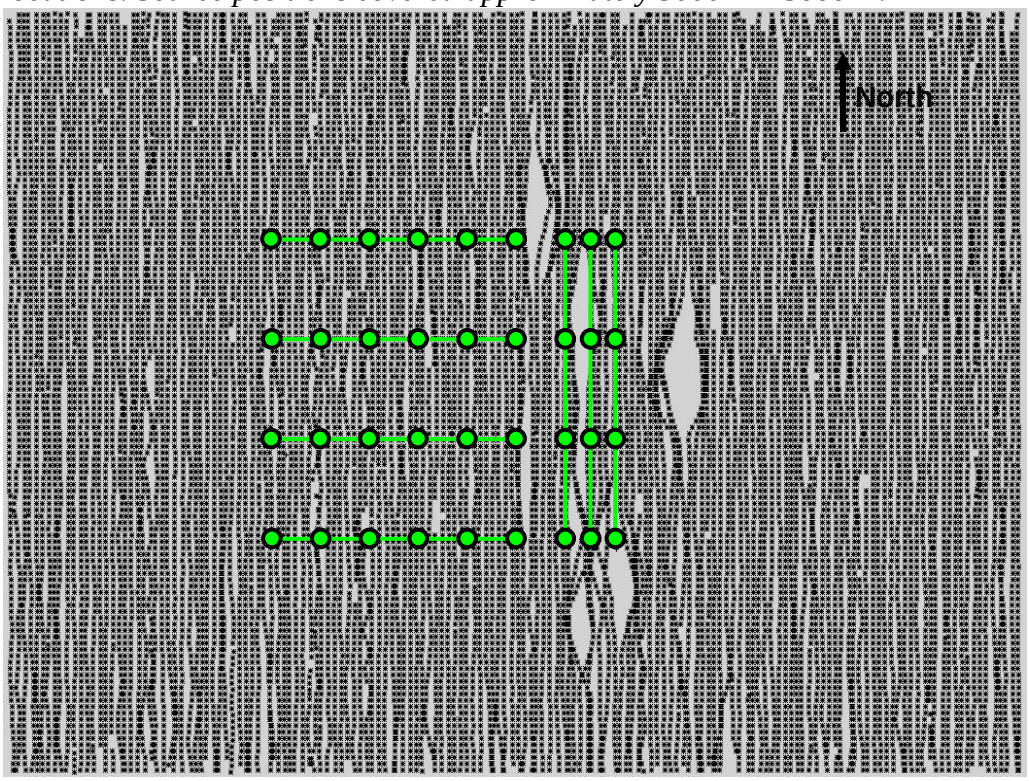


*Figure 3.* ***Phase 2****. Black squares show source positions, green dots show receiver locations. Source positions covered approximately 4000 m x 3000 m.*

Figure 2 was made from Phase 1 data; Figure 3 was made from Phase 2 data.

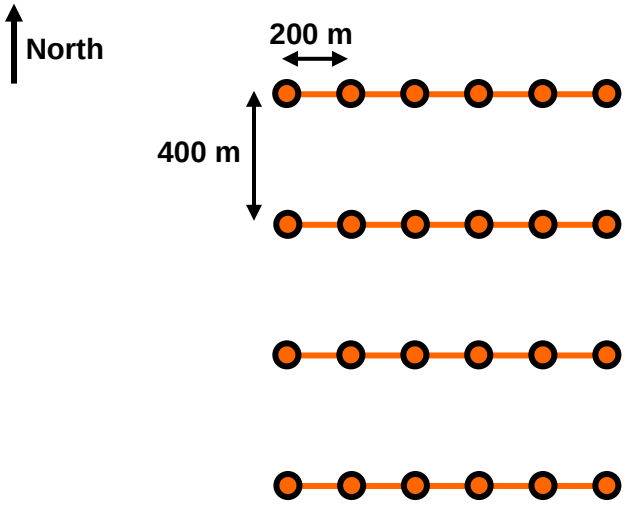


*Figure 4. **Phase 1** acquisition used four cables with six receivers on each cable.*

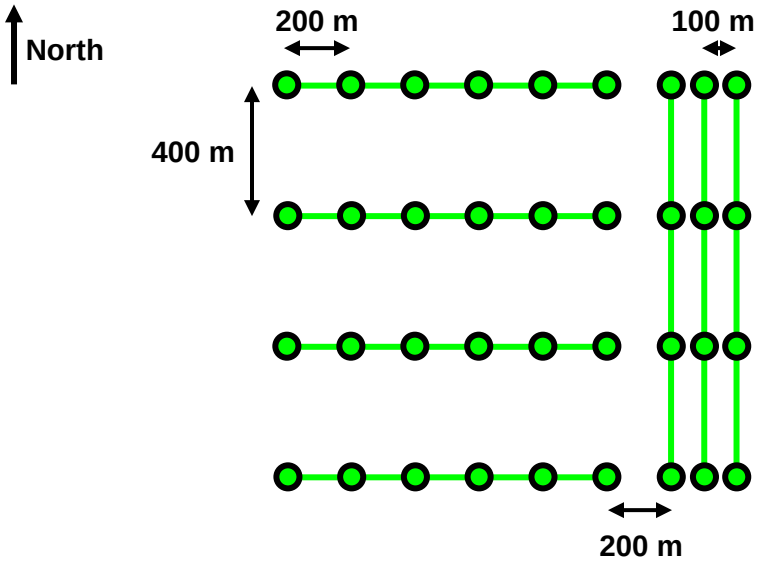


*Figure 5. **Phase 2** acquisition used the original cable locations and added three more cables to the east.*

For Phase 1, the cables were laid on the seafloor. "Sandbags (under license from ARCO) were used to match sensor acoustic impedance to water bottom acoustic impedance; this improved coupling and reduced noise from turbulent flow over the sensors (Ebrom et al., 1998)."

For Phase 2, the four east-west cables and the western north-south cable were buried 1 m under the seafloor, the central north-south cable was laid on the seafloor with sensors

taped to it, and the eastern north-south cable was laid on the seafloor with receivers taped and sandbagged (Rodriguez-Suarez et al., 2000a).

"It was decided to use a source with a highly-repeatable, high-frequency signature, with minimal directionality. The choice was Seascan's 1120-in$^3$ Tricluster array of I/O sleeve guns, which was used at a depth of 3 m. This array's sprung rigid frame maintains its geometry at different towing speeds, and is symmetrical in both the inline and crossline directions (Ebrom et al., 1998)."

Figure 6 provides an overview of the Teal South field. This is a horizon map of the so-called 4500 ft. sand, the "Producer." It was made from Phase 2 PZ far offset stack data. In this case, the offset range is 1282-1800 m (24°-32° at the Producer reservoir). (The "Little Neighbor" reservoir was the subject of another study: Pennington et al., 2001.)

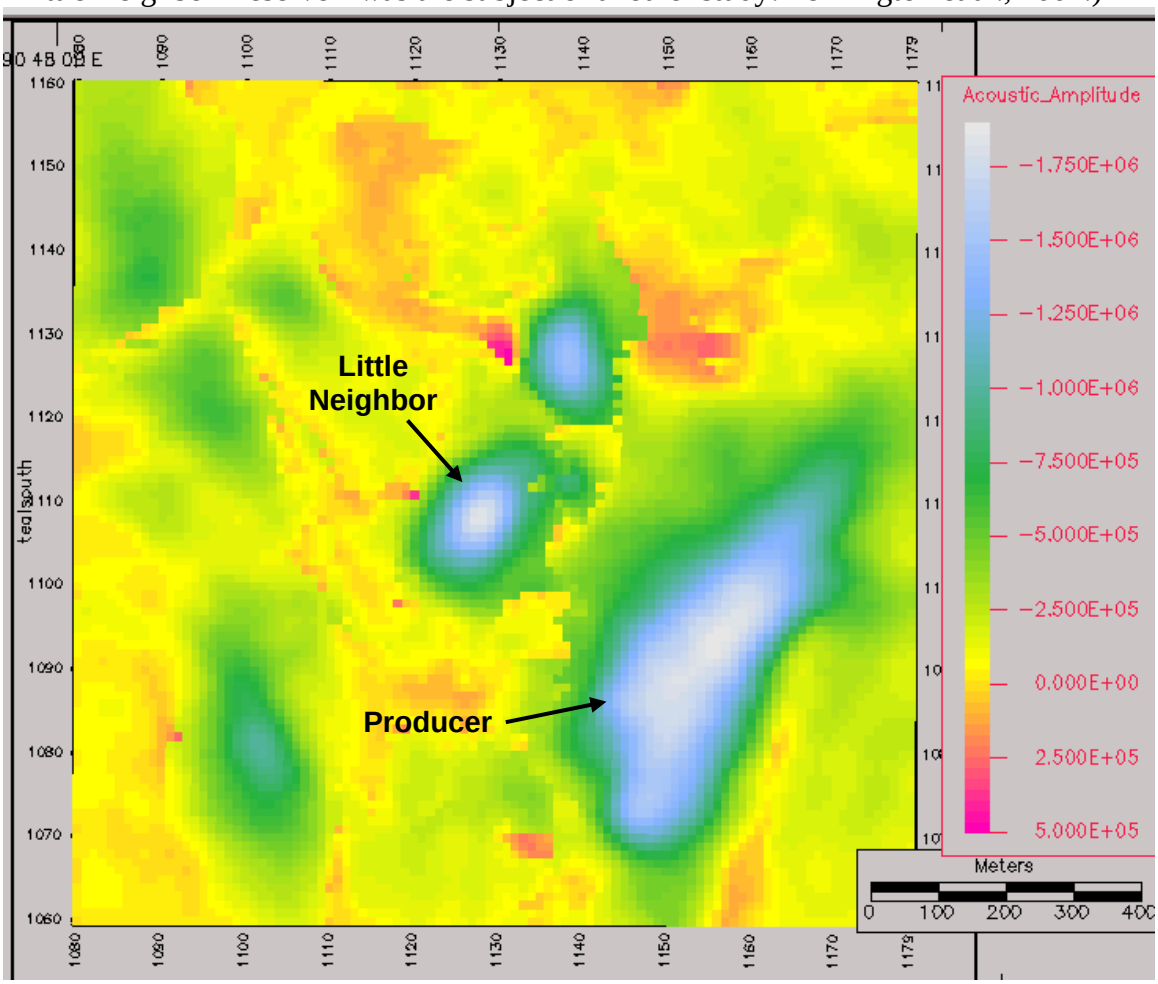


*Figure 6. Teal South 4500 ft. sand horizon map (Acevedo & Pennington, ERCH, Sep. 6, 2001).*

## 2. Multi-component Recording

As stated earlier, 4-component recording means that each receiver position has an inline geophone, a crossline geophone, a vertical geophone, and a hydrophone. Figure 7 shows an example of an ocean bottom receiver that has the three geophones and one hydrophone in one package.

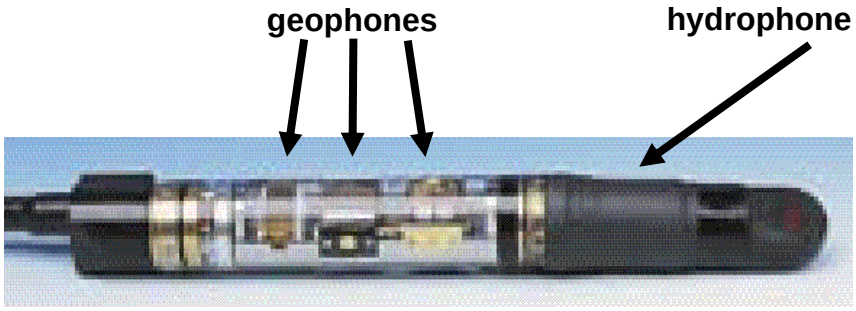


*Figure 7. An example 4-component receiver (image courtesy of Sercel).*

The hydrophone can only record P-waves because S-wave propagation is not supported in fluid.

Idealized for a deep reflector, the vertical (Z) geophone records only P-wave motion and the two horizontal (inline and crossline) geophones record only S-wave motion.

A report (Rodriguez-Suarez et al., 2000a) that studied the quality of the Phase 2 data stated, “There appear to be some contamination of S-wave energy on the vertical channel, but little P-wave energy on the horizontal channel.”

## 3. PP-waves and PS-waves

At each subsurface interface, reflection and refraction occur. At non-normal incidence, P-waves undergo some mode conversion to S-waves, and vice-versa. Energy partitioning is governed by the angle of incidence and elastic properties of the two layers: Vp, Vs, and density ($\rho$) (see Figure 8).

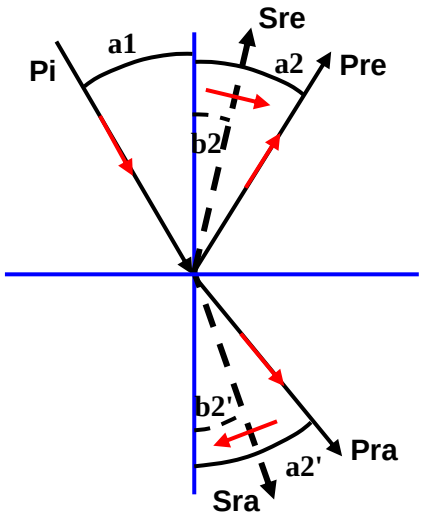


*Figure 8. Energy partitioning diagram for a P-wave incident at the interface of two homogenous isotropic layers. The incident P-wave is in the upper left. Black arrows represent the direction of wave propagation; red arrows represent the direction of energy propagation.*

Figure 9 illustrates shear wave birefringence. When a shear wave enters an azimuthally anisotropic medium, a medium of aligned vertical fractures, it is split into a fast (S1) component, polarized parallel to the fractures, and a slow (S2) component, polarized perpendicular to the fractures.

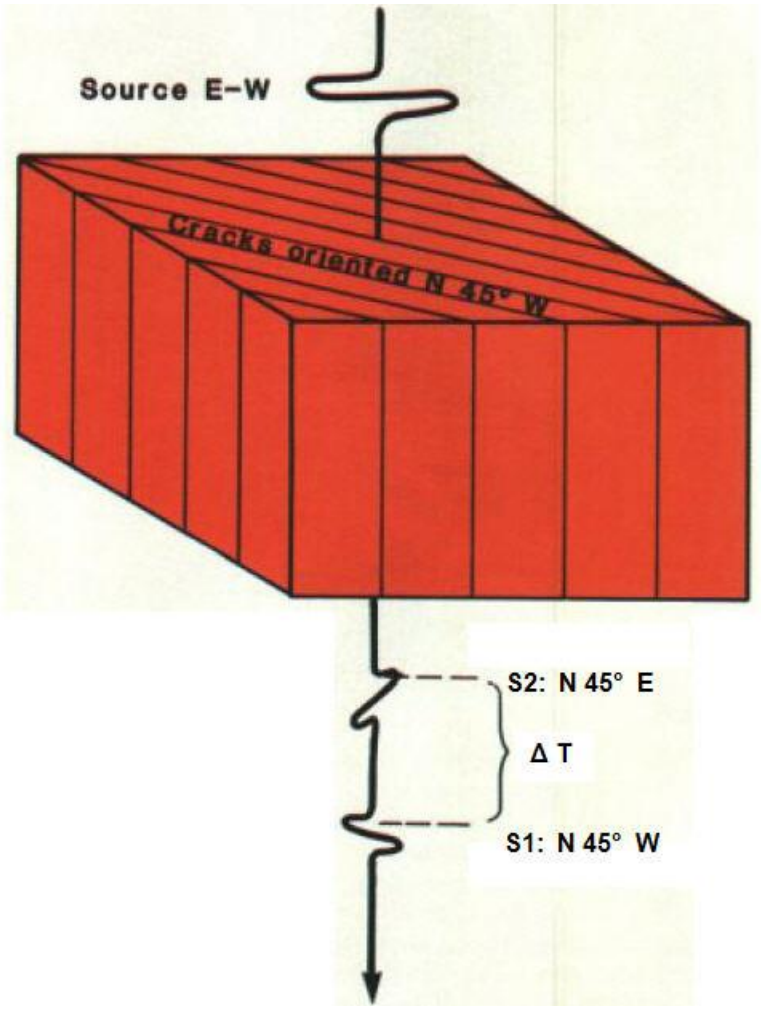


*Figure 9. Model of shear wave birefringence. (After Martin and Davis, 1987.)*

## 4. C-waves

C-waves are the special case of a converted wave in which most of the energy converts from P-wave down to S-wave up only at the reflecting horizon. C-waves are recognized as the dominant form of S-waves from a P-wave source in OBC recording (Rodriguez-Suarez et al., 2000b). In my study field, Teal South, C-wave detection is the purpose of multi-component recording.

Figure 10 shows two reflection scenarios for the same source and receiver pair above homogenous, isotropic, and horizontal layers. The left side of Figure 10 shows that for P-to-P reflections at the same source and receiver, there is a surface point that is a midpoint for all subsurface reflections; that is, a common midpoint (CMP). (Note: This is not the usual definition of CMP.) The right side of Figure 10 shows that for P-to-S reflections, there is no common midpoint. Instead, a "common conversion point" (CCP) can be constructed by following a hyperbola along the reflection points. The CCP hyperbola is asymptotic to the source-receiver midpoint.

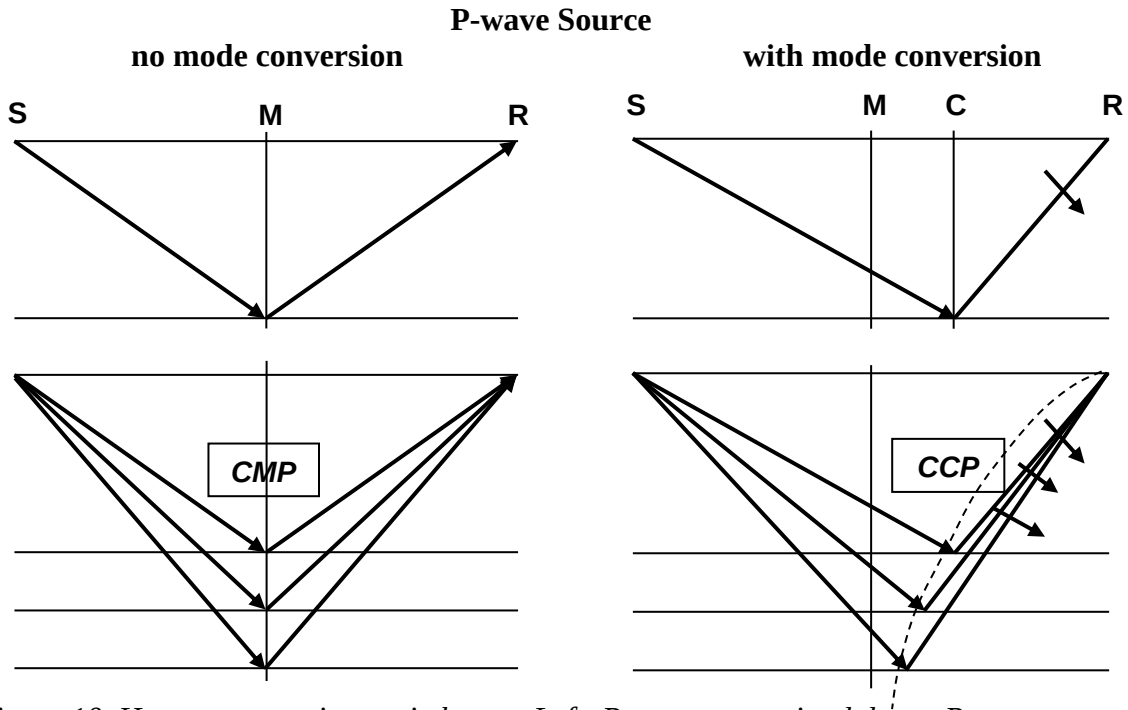


*Figure 10. Homogeneous, isotropic layers. Left: P-wave transmitted down, P-wave reflected up. Right: P-wave transmitted down, S-wave reflected up. S is the source point, R is the receiver point, M is the midpoint between source and receiver, and C is the point of mode conversion.*

## 5. Pre-migration Data Processing

The prestack gathers were processed by CGG. CGG applied the following processes to the PZ prestack gathers:

- Geometry QC, CDP bin grid, trace header updates
- Trace edits
- PZ summation for de-ghost and de-pegleg
- Gain recovery: spherical divergence, 3 dB/sec, offset gain
- Median filter applied in offset domain for random noise bursts
- Receiver gain balancing
- Conical 3D f-k filter applied in receiver domain for linear noise
- CDP sort
- Surface-consistent gapped deconvolution:
    - Predictive length = 35 ms
    - Operator length = 120 ms
- **NMO correction (same correction applied to Phase 1 and Phase 2)**
- Mute
- Automatic statics
- Final bandpass filter:
    - 0-800 ms (8-12-90-120 Hz)
    - 1300-4000 ms (4-8-60-90 Hz)
- Zero-phasing filter

CGG applied the following processes to the PS (C1 and C2) prestack gathers:

- Geometry QC, trace header updates
- Trace edits
- Rotate to C1/C2 (C1 rotated clockwise to 104° from north, C2 rotated clockwise to 14° from north)
- Gain recovery: spherical divergence with offset gain
- Median filter applied in offset domain for random noise bursts
- Receiver gain balancing (single operator per receiver)
- Conical 3D f-k filter applied in receiver domain for linear noise
- Asymptotic CCP binning (Vp/Vs = 2.8)
- CCP sort
- Apply source statics from PZ
- Receiver statics from receiver stack
- Surface-consistent gapped deconvolution:
    - Predictive length = 74 ms
    - Operator length = 280 ms
- **NMO correction**
- Mute
- Automatic statics

All prestack gathers were NMO-corrected (flattened) by CGG (the processing steps above in bold).

The data were acquired using multi-component geophones that were aligned in the inline/crossline directions. As stated above, during processing, the data were rotated from inline/crossline coordinates to C1/C2 (Alford, 1986), the natural coordinate system (Sheriff, 2002) of Teal South. C1/C2 are the converted wave equivalent of S1/S2. The C1 axis is clockwise 104° from north, the C2 axis is clockwise 14° from north (Figure 11).

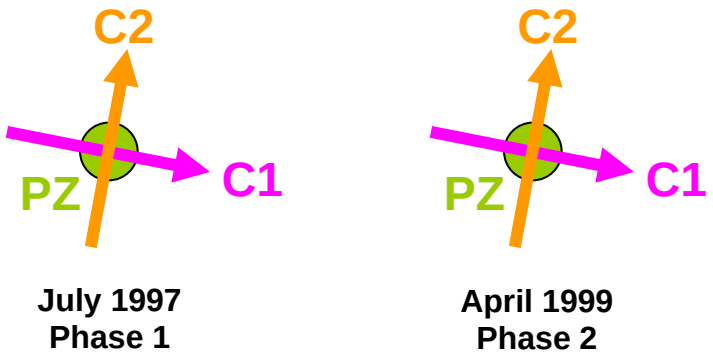


*Figure 11. Schematic map view of the six data sets of prestack gathers after CGG processing.*

Figure 12 shows CGG's polarization analysis that led to their rotation decisions.

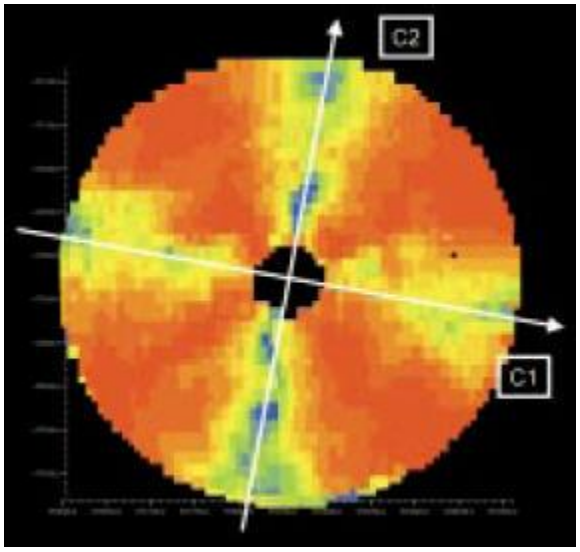


*Figure 12. Amplitude ratio between radial and transverse components in a window between 2500 and 2700 ms in a common geophone gather. (After Spitz, 2001.)*

After contractor processing, there are three datasets of prestack gathers for each Phase: PZ, C1 and C2 (see Figure 11).

## 6. References


Alford, R.M., 1986, Shear data in the presence of azimuthal anisotropy: Dilley, Texas: 56th Annual International Meeting, SEG, Expanded Abstracts, 476-479.

Ebrom, D., P. Krail, D. Ridyard, and L. Scott, 1998, 4-C/4-D at Teal South: The Leading Edge, **17**, 1450-1453.

Martin, M.A., and T.L. Davis, 1987, Shear-wave birefringence: A new tool for evaluating fractured reservoirs: The Leading Edge, 6, 22-28.

Pennington, W.D., H. Acevedo, J.I. Haataja, and A. Minaeva, 2001, Seismic time-lapse surprise at Teal South: That little neighbor reservoir is leaking!: The Leading Edge, **20**, 1172-1175.

Rodriguez-Suarez, C., R.R. Stewart, and H.-X. Lu, 2000a, Analysis of the Teal South, Gulf of Mexico, 3D-4C seismic survey: 70th Annual International Meeting, SEG, Expanded Abstracts, .1150-1153

Rodriguez-Suarez, C., R.R. Stewart, and G.F. Margrave, 2000b, Where does S-wave energy on OBC recordings come from?: 70th Annual International Meeting, SEG, Expanded Abstracts, 1170-1173.

Sheriff, R.E., 2002, Encyclopedic Dictionary of Applied Geophysics: Society of Exploration Geophysicists.

Spitz, S., W. Haggard, and P. Harris, 2001, Teal South: the first 4D-4C: CGG World, **32**, 17-18.

## Appendix A. Stacking Velocities

To migrate stacked volumes of near offsets and far offsets, I used stacking velocities supplied by CGG. The stacking velocities that I actually used (below) differ slightly from those in the supplied velocity files: I added a first T-V pair that repeats the first velocity at zero time and I added a last T-V pair that repeats the last velocity at the last time of the data set. I did this to avoid velocity interpolation errors at beginning and end times. Figure A.1 shows only the original T-V values.

The PZ inline/crossline pair are 1104/1144. The PS inline/crossline pair are 1104/1128.

The line breaks in A.2 and A.3 emphasize that Phase 1 CCP velocity analysis was slightly more detailed than Phase 2 CCP velocity analysis. There are three T-V pairs between the line breaks in Phase 1 compared to one T-V pair between the line breaks in Phase 2. Otherwise, T-V pairs in both sets are almost identical.

### *A.1. Stacking velocities applied to Phase 1 & 2 PZ CDP gathers*

| Inline | Xline | Time (ms) | Velocity (m/s) |
|---|---|---|---|
| 1104 | 1144 | 0 | 1436 |
| 1104 | 1144 | 25 | 1436 |
| 1104 | 1144 | 225 | 1586 |
| 1104 | 1144 | 325 | 1679 |
| 1104 | 1144 | 450 | 1731 |
| 1104 | 1144 | 625 | 1768 |
| 1104 | 1144 | 825 | 1845 |
| 1104 | 1144 | 975 | 1922 |
| 1104 | 1144 | 1150 | 2002 |
| 1104 | 1144 | 1400 | 2028 |
| 1104 | 1144 | 1700 | 2054 |
| 1104 | 1144 | 1875 | 2062 |
| 1104 | 1144 | 2025 | 2046 |
| 1104 | 1144 | 2275 | 2021 |
| 1104 | 1144 | 2500 | 2078 |
| 1104 | 1144 | 2750 | 2124 |
| 1104 | 1144 | 3125 | 2209 |
| 1104 | 1144 | 3525 | 2533 |
| 1104 | 1144 | 3750 | 2732 |
| 1104 | 1144 | 4000 | 2732 |

### *A.2. Stacking velocities applied to Phase 1 C1 & C2 CCP gathers*

| Inline | Xline | Time (ms) | Velocity (m/s) |
|---|---|---|---|
| 1104 | 1128 | 0 | 821 |
| 1104 | 1128 | 25 | 821 |
| 1104 | 1128 | 325 | 757 |
| 1104 | 1128 | 475 | 699 |
| 1104 | 1128 | 875 | 762 |
| 1104 | 1128 | 1250 | 807 |
| 1104 | 1128 | 1525 | 867 |
| 1104 | 1128 | 1875 | 932 |
| 1104 | 1128 | 2125 | 977 |
| 1104 | 1128 | 2425 | 1036 |
| 1104 | 1128 | 2650 | 1072 |
| 1104 | 1128 | 2875 | 1107 |
| 1104 | 1128 | 3125 | 1157 |
| 1104 | 1128 | 3375 | 1186 |
| 1104 | 1128 | 3600 | 1249 |
| 1104 | 1128 | 4000 | 1269 |
| 1104 | 1128 | 4750 | 1540 |
| 1104 | 1128 | 6000 | 1540 |

### *A.3. Stacking velocities applied to Phase 2 C1 & C2 CCP gathers*

| Inline | Xline | Time (ms) | Velocity (m/s) |
|---|---|---|---|
| 1104 | 1128 | 0 | 821 |
| 1104 | 1128 | 25 | 821 |
| 1104 | 1128 | 325 | 757 |
| 1104 | 1128 | 475 | 699 |
| 1104 | 1128 | 875 | 762 |
| 1104 | 1128 | 1250 | 807 |
| 1104 | 1128 | 1525 | 867 |
| 1104 | 1128 | 1875 | 940 |
| 1104 | 1128 | 2125 | 977 |
| 1104 | 1128 | 2425 | 1036 |
| 1104 | 1128 | 2650 | 1072 |
| 1104 | 1128 | 2950 | 1119 |
| 1104 | 1128 | 3600 | 1249 |
| 1104 | 1128 | 4000 | 1269 |
| 1104 | 1128 | 4750 | 1540 |
| 1104 | 1128 | 6000 | 1540 |

### *A.4. Time versus velocity chart of stacking velocities*

Examining the PS time-velocity pairs, one sees that the Phase 1 (magenta) and Phase 2 (blue) data sets quite nearly overlap.

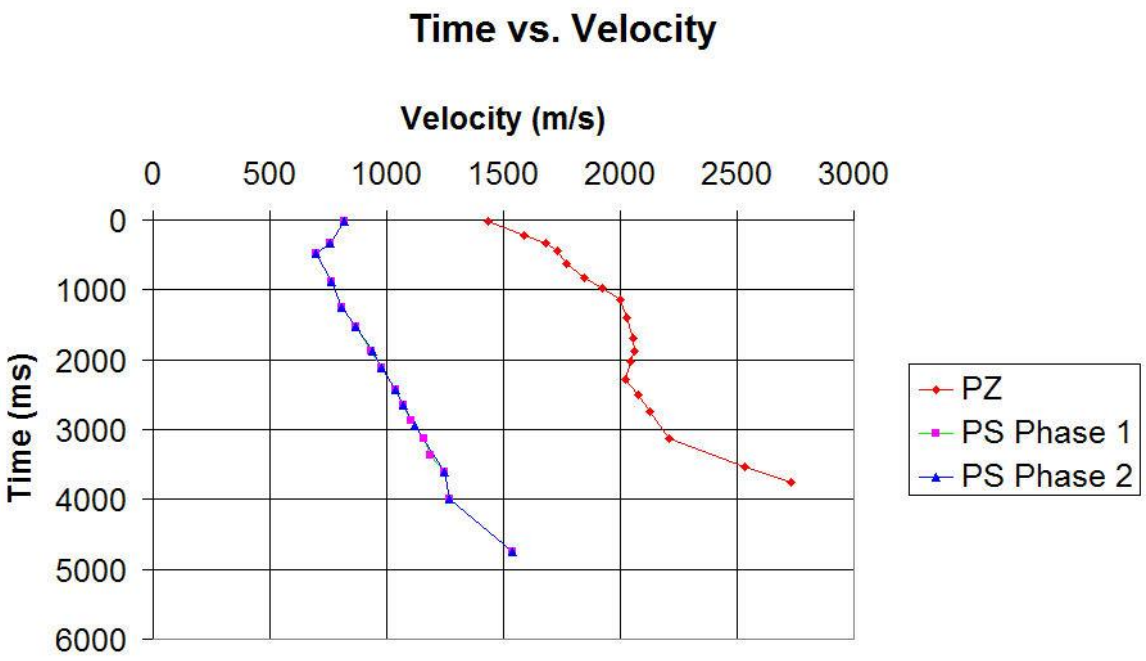


*Figure A.1. Time-velocity pairs for both PZ data sets (identical) at inline/crossline 1104/1144, and time-velocity pairs for Phase 1 PS and Phase 2 PS at inline/crossline 1104/1128.*